# Contrast and Error-Based Fusion Schemes for Multispectral Image Pansharpening

Gemine Vivone, Rocco Restaino, Mauro Dalla Mura, *Member, IEEE*, Giorgio Licciardi, *Member, IEEE*, and Jocelyn Chanussot, *Fellow, IEEE*

***Abstract*—The pansharpening process has the purpose of building a high-resolution multispectral image by fusing low spatial resolution multispectral and high-resolution panchromatic observations. A very credited method to pursue this goal relies upon the injection of details extracted from the panchromatic image into an upsampled version of the low-resolution multispectral image. In this letter, we compare two different injection methodologies and motivate the superiority of contrast-based methods both by physical consideration and by numerical tests carried out on remotely sensed data acquired by IKONOS and Quickbird sensors.**

***Index Terms*—High pass modulation, injection models, modulation transfer functions, pansharpening.**

## I. Introduction

NARROW spectral bandwidth and high spatial resolution represent two desirable, but conflicting requirements, for any real remote sensor. A step toward the achievement of both these characteristics can be taken by jointly employing data acquired by multiple sensors with different spatial and spectral resolutions. For example, this procedure is applied to the enhancement of multispectral (MS) images by exploiting a higher spatial resolution PANchromatic (PAN) image of the same scene, both usually acquired from the same platform.

The described process is known as Pansharpening and aims at increasing the spatial resolution of a multispectral image, here denoted as $\mathbf{MS}$, by using a companion panchromatic image, hereafter indicated by $\mathbf{P}$. The output of the fusion procedure is $\widehat{\mathbf{MS}}$, an estimate of $\mathbf{HRMS}$, which is the real high spatial resolution version of $\mathbf{MS}$ used (when available) as the reference image. In general the pansharpening is carried out by injecting the spatial details contained in $\mathbf{P}$ (and not resolved by the $\mathbf{MS}$) into an upsampled version of $\mathbf{MS}$ [1], [2]. This very diffused approach is based on two sequential phases: i) the extraction of the high-resolution details from $\mathbf{P}$ and ii) their injection into $\mathbf{MS}$. In this letter we focus on the second aspect by highlighting the central role that the sensor modulation transfer function (MTF) plays in this step.

The characteristics that $\widehat{\mathbf{MS}}$ should have are formalized by the Wald protocol [1]. This, in addition to the preservation of the spectral characteristics of $\mathbf{MS}$, prescribes how the pansharpening algorithm has to be designed for properly bringing the $\mathbf{MS}$ to the spatial resolution of the $\mathbf{P}$. The term *spatial resolution* refers to the capability of resolving objects in the scene and it depends on the blurring introduced by the imaging system during the acquisition. Essentially, the sensors can be approximated as a nonideal optical systems whose effect can be considered as the output of a linear stationary model. In these terms, the acquisition system can be fully characterized by means of its spatial impulse response, named *Point Spread Function* (*PSF*) [3]. In this letter we leverage on this aspect and we explicitly express the pansharpening objective of having the same spatial resolution for both the $\mathbf{P}$ and the enriched $\mathbf{MS}$ by imposing the following equality:

$$\mathbf{PSF}_{\widehat{\mathbf{MS}}} = \mathbf{PSF}_{\mathbf{P}}. \tag{1}$$

We recall that $\mathcal{F}\{\mathbf{PSF}\}$, the frequency representation of the PSF, is defined as the product of the MTF and the phase transfer function (PTF), which are, respectively the modulus and the phase of the PSF in the Fourier domain. The equality in (1) can be approximated by matching the MTFs in the frequency domain, since the modulus of the PSF constitutes the main contribution to the overall response of the acquisition system [4].

The main contributions of this letter are i) the analysis of the injection methods for pansharpening in the light of (1) and ii) the expression of the constraint on the matching of the MTFs in terms of image local contrast. Furthermore, the findings presented in this work can be related to rather more general image fusion contributions, that already highlighted the superiority of methods based on contrast pyramids [5]. Focusing on the pansharpening applications, the same considerations justify the very appealing visual features of the *high pass modulation* (HPM) method, that have been often claimed in the recent literature [6].

The letter is organized as follows: Section II presents the importance of the MTF in pansharpening and highlights its links with the image contrast. In Section III two methods for the extraction of details are introduced and used for the comparison reported in Section IV. Finally, Section V presents the final remarks and perspectives.

Manuscript received July 3, 2013; revised August 24, 2013; accepted September 11, 2013.

G. Vivone and R. Restaino are with the Departmant of Information Engineering, Electrical Engineering and Applied Mathematics, (DIEM), University of Salerno, 84084 Salerno, Italy (e-mail: gvivone@unisa.it; restaino@unisa.it).

M. Dalla Mura and G. Licciardi are with the GIPSA-Lab, Grenoble Institute of Technology, 38000 Grenoble, France (e-mail: mauro.dalla-mura@gipsa-lab.grenoble-inp.fr; giorgio-antonino.licciardi@gipsa-lab.grenoble-inp.fr).

J. Chanussot is with the GIPSA-Lab, Grenoble Institute of Technology, 38000 Grenoble, France, and also with the Faculty of Electrical and Computer Engineering, University of Iceland, 101 Reykjavik, Iceland (e-mail: jocelyn.chanussot@gipsa-lab.grenoble-inp.fr).

Color versions of one or more of the figures in this paper are available online at http://ieeexplore.ieee.org.

Digital Object Identifier 10.1109/LGRS.2013.2281996

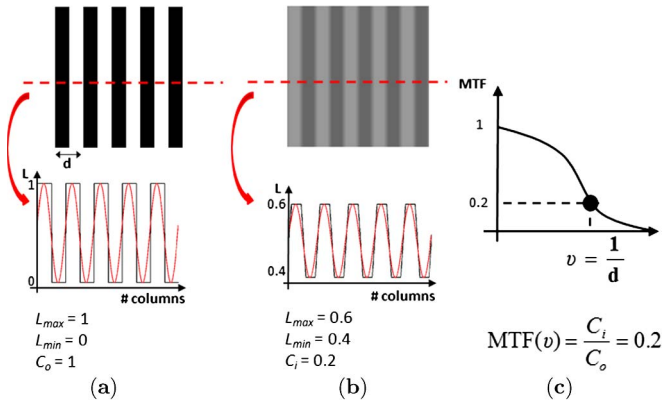


Fig. 1. Example of estimation of the MTF at a given frequency $\nu$ according to (4). (a) Periodic pattern (specimen) at frequency $\nu$, (b) resulting image as acquired by the optical system, and (c) estimation of the MTF at frequency $\nu$.

## II. MTF-Preserving Injection Methods

The goal of this letter is to explore the possibility of obtaining the desired spatial properties in $\widehat{\mathbf{MS}}$ by mimicking the response of the PAN sensor. More in detail we focus on the MTF and propose its use for driving the design of the pansharpening algorithms. Starting from (1) we impose for all bands $b = 1, \ldots, B$ of the $\mathbf{MS}$ the equality

$$\mathrm{MTF}_{\widehat{\mathbf{MS}}^b}(\nu) = \mathrm{MTF}_{\mathbf{P}}(\nu) \tag{2}$$

where $\nu$ refers to the spatial frequency.

The MTF is defined as

$$\mathrm{MTF}(\nu) = \left.\frac{C_i}{C_o}\right|_{o=s(\nu)} \tag{3}$$

where $C_o$ is the contrast of the target object $o$ and $C_i$ the contrast measured from the image of the object acquired by the optical system, both typically normalized by the modulation at zero frequency. Let us recall that according to Michelson [7], the contrast $C$, denoted also as *modulation*, is

$$C = \frac{L_{\max} - L_{\min}}{L_{\max} + L_{\min}} \tag{4}$$

where $L_{\max}$ and $L_{\min}$ are the maximum and minimum luminance (or equivalently radiance when considering radiometric measures) in the pattern, respectively. Fig. 1 shows an example of the practical estimation of the MTF [Fig. 1(c)] at a given frequency $\nu$, performed by computing the contrast according to (4) on the object [Fig. 1(a)] and acquired image [Fig. 1(b)], by employing a binary square wave with fundamental period $d = \nu^{-1}$. By considering several specimens $o(\nu)$ with differing spatial frequencies $\nu$, it can be shown that the image modulation varies as a function of the spatial frequency. Consequently, (2) can be rewritten as

$$\frac{C_{\widehat{\mathbf{MS}}}}{C_o} = \frac{C_{\mathbf{P}}}{C_o} \tag{5}$$

that implies the relation between the contrast of $\mathbf{P}$ and $\widehat{\mathbf{MS}}$ images to be

$$C_{\widehat{\mathbf{MS}}} = C_{\mathbf{P}}. \tag{6}$$

When dealing with real acquisitions, the imaged scenes are typically composed by small objects on a background of uniform luminance [3]. In that case the peak luminance is that of the object to resolve, say $L$, and the mean luminance coincides with that of the background, say $L_b$. In this scenario, the contrast can be computed by *Weber's formula* [8] as

$$C = \frac{L - L_b}{L_b} = \frac{L}{L_b} - 1. \tag{7}$$

This transforms the contrast equality (6) into the relationship, holding for all bands $b = 1, \ldots, B$

$$\frac{\widehat{\mathbf{MS}}^b}{\widehat{\mathbf{MS}}^b_{LP}} - \mathbf{I} = \frac{\mathbf{P}}{\mathbf{P}_{LP}} - \mathbf{I} \tag{8}$$

with $\mathbf{I}$ the identity matrix, $\widehat{\mathbf{MS}}_{LP}$ and $\mathbf{P}_{LP}$ the background luminance of $\widehat{\mathbf{MS}}$ and $\mathbf{P}$, respectively. The first can be computed by degrading the original image with a low-pass filter (thus, the subscript LP), which might be different for each band $b$. According to the Wald protocol, the low-pass version of $\widehat{\mathbf{MS}}$ is constituted by the original MS image and thus (2) turns into the well-known HPM formulation [6]

$$\widehat{\mathbf{MS}}^b = \widetilde{\mathbf{MS}}^b \cdot \frac{\mathbf{P}}{\mathbf{P}_{LP}} \tag{9}$$

in which $\widetilde{\mathbf{MS}}$, an upsampled version of $\mathbf{MS}$, is used for guaranteeing the compatibility of the image sizes. Equation (9) characterizes the fusion methods employing ratio of low-pass decompositions (ROLP), whose superiority with respect to difference of low-pass (DOLP) approaches that are based on the formula

$$\widehat{\mathbf{MS}}^b = \widetilde{\mathbf{MS}}^b + (\mathbf{P} - \mathbf{P}_{LP}) \tag{10}$$

has been proven in [5].

By defining the details $\mathbf{D}$ of the PAN image as

$$\mathbf{D} = \mathbf{P} - \mathbf{P}_{LP}. \tag{11}$$

Equation (9) can also be rewritten as

$$\widehat{\mathbf{MS}}^b = \widetilde{\mathbf{MS}}^b + \frac{\widetilde{\mathbf{MS}}^b}{\mathbf{P}_{LP}}\mathbf{D}. \tag{12}$$

This highlights the inclusion of the HPM method into the general injection model

$$\widehat{\mathbf{MS}}^b = \widetilde{\mathbf{MS}}^b + \alpha^b \mathbf{D} \tag{13}$$

where $\alpha^b$, for $b = 1, \ldots, B$, are the modulation coefficients that weigh the contribution of $\mathbf{P}$. Noticeably, the model (13) can be designed to satisfy a very interesting property: if the low-pass image $\mathbf{P}_{LP}$ used in the calculation of $\alpha^b$ does not depend on $b$, this algorithm belongs to the *spectral distortion minimization* (*SDM*) class, or in other words the pansharpened image $\widehat{\mathbf{MS}}$ exhibits the same spectral distortion of $\widetilde{\mathbf{MS}}$ [9]. However, this property that turns out to be useful in showing the preservation of a crucial spectral feature of $\widetilde{\mathbf{MS}}$, does not necessarily imply

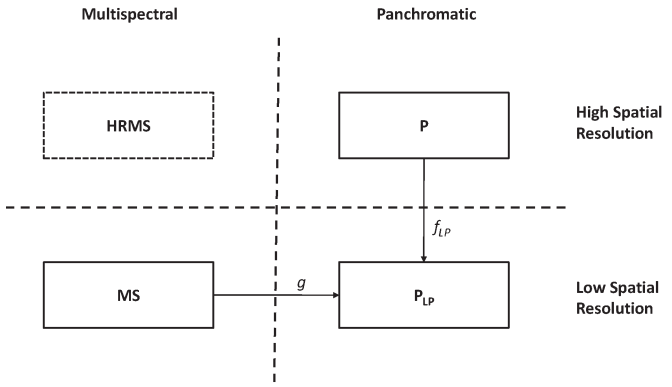


Fig. 2. Images involved in the pansharpening process, arranged according to their spatial and spectral characteristics.

an acceptable quality of the fusion product and has thus to be considered as a secondary requirement for the algorithm design. Indeed, increasing the quantity of the injected details typically implies the increase of spectral distortion [10], that on the contrary could trivially be eliminated by neglecting any contribution of $\mathbf{P}$.

## III. Details Extraction Methods

In the following the experimental results performed on different data sets and with different types of detail extraction algorithms will be presented aiming at showing the very appealing features of pansharpening methods based on (9) with respect to approaches employing formula (10). Two different methods for estimating the required low-pass version $\mathbf{P}_{LP}$ of the PAN image will be considered. One is based on the combination of the available MS images and the other on a proper degradation of the original PAN data.

The two detail injection algorithms can be combined with many different methods for achieving the low-pass image $\mathbf{P}_{LP}$. As illustrated by Fig. 2, they can be grouped in two main categories: one that considers the combination of all the $B$ available bands and the other that is based on the transformation of the full resolution PAN image $\mathbf{P}$.

The first approach (commonly used in *component substitution* (CS) methods) aims at deriving the required low-pass image $\mathbf{P}_{LP}$ by arranging the MS bands through a function $g$

$$\mathbf{P}_{LP} = g(\mathbf{MS}^1, \ldots, \mathbf{MS}^B). \tag{14}$$

Knowledge about the used sensor can be helpful to estimate $g$. Unfortunately $g$ is scarcely available in practice since it is typically neither provided by the sensors' constructors nor derived analytically [11]. So it should be estimated from the data (usually under hypothesis of linearity of $g$). The simplest algorithm for estimating $g$, is the fast IHS (FIHS) [10] in which the PAN image is obtained by averaging all multispectral bands, or in other terms by adopting the assumption (hardly verified in the practice) that the MS bands equally contribute to the PAN image. Furthermore, the FIHS method employs (10) for the injection of details [12]. The corresponding contrast-based method using (9) is named Brovey [12].

In the second approach the low-pass version $\mathbf{P}_{LP}$ is constructed from the PAN image $\mathbf{P}$ by applying a properly chosen transformation $f_{LP}(\cdot)$, namely obtained as

$$\mathbf{P}_{LP} = f_{LP}(\mathbf{P}). \tag{15}$$

A straightforward implementation consists in applying a high pass filter (HPF) for extracting details from the PAN image. The best results can be achieved by considering a system with complementary frequency responses with respect to the MTF of the sensor, whose shape can be safely approximated by a Gaussian function. This technique, referred in this letter to as *MTF method*, was first proposed in [4] and successively efficiently implemented through the HPM details injection scheme (9) in [6].

A more sophisticated way for building the $\mathbf{P}_{LP}$ image consists in utilizing a *multiresolution analysis* (*MRA*) [13], which aim at separating the informative content at the various spatial scales. In this scheme, starting from the original image $\mathbf{P}$, a sequence of low-pass version (called approximations) obtained with progressively reduced cut off frequency is constructed through repeated applications of an *analysis operator*. The image at the lowest scale coincides with the required image $\mathbf{P}_{LP}$. In particular, we chose for the comparison of the two injection methods a Wavelet implementation based on the *á trous filters*, that allows to design the analysis operator so that the equivalent low-pass filter matches the sensor MTF [14]. In the same reference an HPM implementation, satisfying the SDM requirement has been utilized, while an Á Trous Wavelet Trasform (ATWT) technique employing an additive model for details injection was previously proposed in [15].

## IV. Experimental Results

Two of the most popular sensors for pansharpening applications are IKONOS and QuickBird. They work in the visible and near infrared spectrum range with the MS sensor that is characterized by four bands (blue, green, red and NIR) and they also have a PAN channel. The spatial resolution of IKONOS is $4 \times 4$ m for the MS bands and $1 \times 1$ m for the PAN. QuickBird has an asymmetric pixel. Indeed, the resolution cell for the multispectral bands is $2.44 \times 2.88$ m, while for the PAN channel is $0.61 \times 0.72$ m. The experimental results have been conducted on two real data sets.[1] In particular, we selected a scene of the China-Sichuan region (called China data set, Fig. 3) and a region of India (called India data set, Fig. 4) acquired by the IKONOS and Quickbird sensors, respectively.

A quantitative analysis is performed by considering a reference image according to the Wald's protocol [1]. Namely both the PAN and MS images are spatially degraded and the pansharpening algorithms are applied to the synthetically degraded images; the original MS image then is considered as reference for assessing the quality of the methods. The low-resolution MS bands (four times lower than that of the PAN image) are obtained by applying a low-pass filtering and decimation [16]. The frequency response of the low-pass filter is designed to match the MTF of each spectral channel of the sensor and the panchromatic channel is degraded by means of an ideal low-pass filtering [4], [6].

[1] Available at http://glcf.umiacs.umd.edu.

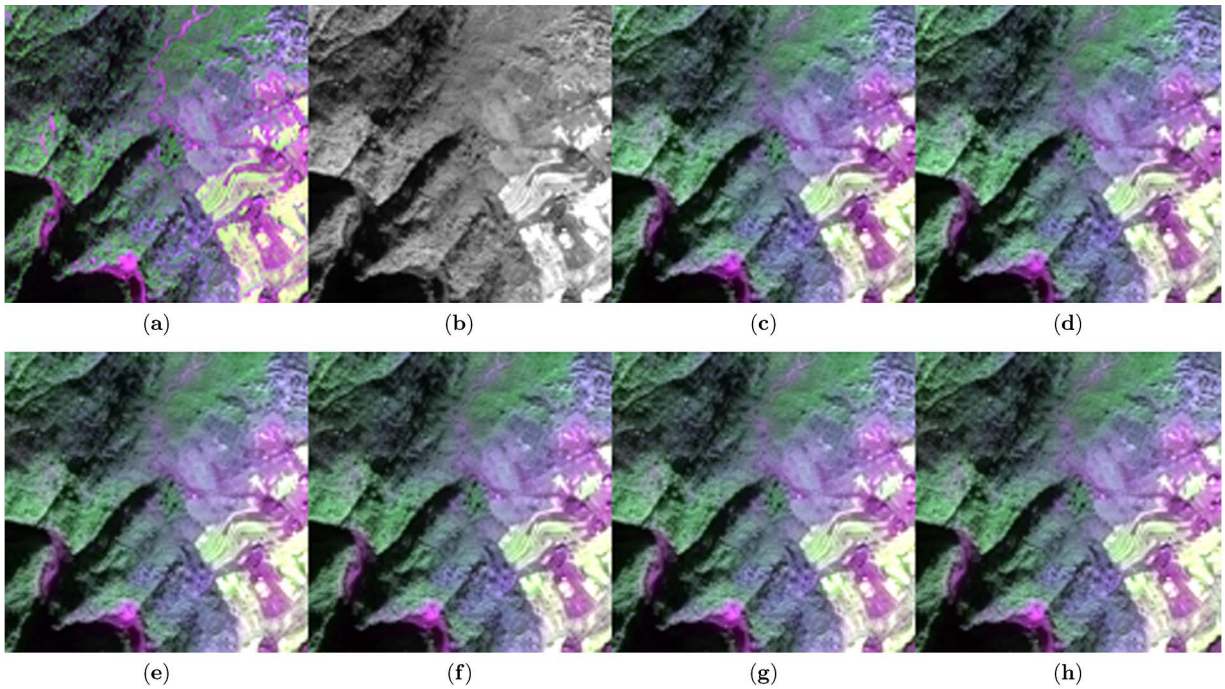


Fig. 3. China data set false color representation (NIR, red, and green): (a) full resolution MS image (reference); (b) PAN image; (c) GIHS-ERR (FIHS); (d) GIHS-CON (Brovey); (e) MTF-ERR; (f) MTF-CON; (g) ATWT-ERR; (h) ATWT-CON.

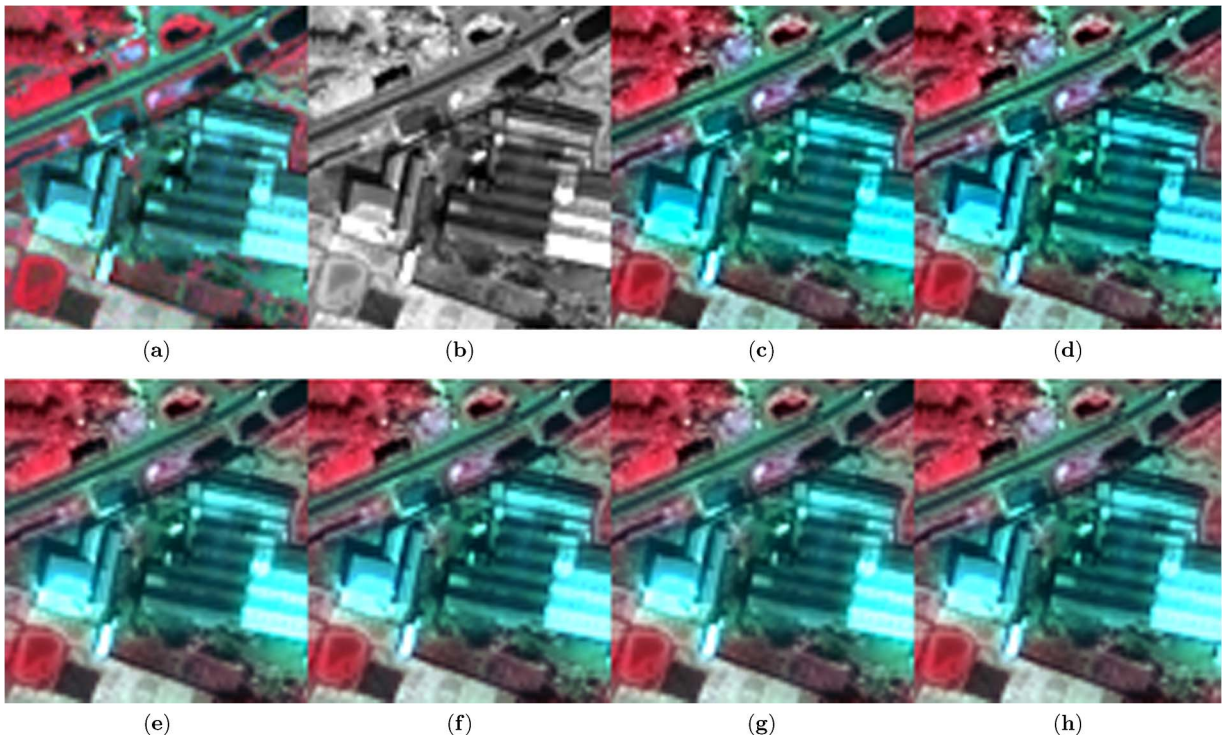


Fig. 4. India data set false color representation (NIR, red, and green): (a) full resolution MS image (reference); (b) PAN image; (c) GIHS-ERR (FIHS); (d) GIHS-CON (Brovey); (e) MTF-ERR; (f) MTF-CON; (g) ATWT-ERR; (h) ATWT-CON.

The assessment of the fused products (with respect to the reference image) is carried out by calculating different indexes [16] such as the *Q4 index* [17] and the *ERGAS* [13] to evaluate the global quality of images. The spectral and spatial distortions are assessed by the *spectral angle mapper* (*SAM*) and the *spatial correlation coefficient* (*SCC*) [18], respectively. We recall that the optimal values of the indexes are one for Q4 and SCC and zero for ERGAS and SAM.

The numerical results achieved by contrast-based (CON) and error-based (ERR) injection methods (Section III) on the China and India data sets are reported in Tables I and II.

TABLE I
COMPARISON BETWEEN ERROR-BASED (ERR) AND CONTRAST-BASED (CON) INJECTION MODELS: CHINA DATASET

| | Injection | Q4 | SAM(°) | ERGAS | SCC |
|---|---|---|---|---|---|
| GIHS | ERR | 0.8512 | 3.5836 | 2.8178 | 0.9069 |
| | CON | 0.8528 | 3.4985 | 2.7788 | 0.9102 |
| MTF | ERR | 0.8763 | 3.2425 | 2.6207 | 0.9022 |
| | CON | 0.8792 | 3.1872 | 2.5801 | 0.9059 |
| ATWT | ERR | 0.8767 | 3.1973 | 2.6058 | 0.9042 |
| | CON | 0.8800 | 3.1272 | 2.5600 | 0.9083 |

TABLE II
COMPARISON BETWEEN ERROR-BASED (ERR) AND CONTRAST-BASED (CON) INJECTION MODELS: INDIA DATASET

| | Injection | Q4 | SAM(°) | ERGAS | SCC |
|---|---|---|---|---|---|
| GIHS | ERR | 0.7450 | 3.2976 | 2.1561 | 0.9074 |
| | CON | 0.7484 | 3.1214 | 2.1064 | 0.9162 |
| MTF | ERR | 0.8373 | 2.7817 | 1.7109 | 0.9097 |
| | CON | 0.8451 | 2.7212 | 1.6581 | 0.9158 |
| ATWT | ERR | 0.8338 | 2.8112 | 1.7262 | 0.9091 |
| | CON | 0.8421 | 2.7507 | 1.6705 | 0.9154 |

The superiority of the CON model is evident in all the considered scenarios and to a different extent for all kinds of algorithms. All the quality indexes are improved by this choice, but a finer analysis reveals that the use of (9) allows to reduce some typical drawbacks of CS and MRA details extraction methodologies. Indeed the CS methods are known to be affected by a more significant spectral distortion that is in part compensated by the CON method, as testified by the enhancement achieved by the SAM index. On the other side the MRA methods benefit from the use of rule (9) especially in terms of SCC index, indicating a substantial contribution in terms of spatial details.

Visual analysis can be performed by Figs. 3 and 4 in which two magnified parts of the considered data set have been shown in false colors (NIR, red, and green). In both cases the inspection corroborates the considerations derived during the analysis of quantitative parameters. In particular, the superior spectral quality of images achieved by the CON paradigm in the GIHS approach [Figs. 3(d) and 4(d)] with respect to those attained by the same CS method with ERR injection rule [Figs. 3(c) and 4(c)] can be observed by comparing the fused products with the reference images reported in Figs. 3(a) and 4(a). The presence of additional details in images obtained by the CON rule can be noted in the corresponding images of Fig. 4.

Finally, it is worth noticing that among the algorithms used for the current analysis the ATWT and MTF methods compare favorably in all the test cases. Indeed, these approaches utilizing a filter designed to match the sensor MTF takes advantage with respect to the other competitors from a more proper details extraction phase.

## V. CONCLUSION

In this letter, we have shown that, considering the physics of acquisition systems, the injection of the high spatial resolution details of the panchromatic image into low-resolution MS images can be accurately achieved by imposing the equality between the MTFs of the PAN and the estimated HRMS image. This approach constitutes a step toward the construction of a synthetic MS image with the same spatial resolution of the PAN image fulfilling the Wald protocol. The method has been applied to both CS- and MRA-based pansharpening methods. The experimental analysis confirmed the capability of the proposed HPM details injection paradigm for improving the quality of the fused product based on both approaches and proved its superiority with respect to error based injection schemes. The main research topic arising from this study will focus on the definition of methods for optimally extracting the details from the PAN image.

## REFERENCES


[1] L. Wald and T. Ranchin, "Fusion of satellite images of different spatial resolutions: Assessing the quality of resulting images," *Photogram. Eng. Remote Sens.*, vol. 63, no. 6, pp. 691–699, Jun. 1997.

[2] A. Garzelli, F. Nencini, and L. Capobianco, "Optimal MMSE pan sharpening of very high resolution multispectral images," *IEEE Trans. Geosci. Remote Sens.*, vol. 46, no. 1, pp. 228–236, Jan. 2008.

[3] R. Schowengerdt, *Remote Sensing: Models and Methods for Image Processing*, 3rd ed. Amsterdam, The Netherlands: Elsevier, 2007.

[4] B. Aiazzi, L. Alparone, S. Baronti, A. Garzelli, and M. Selva, "MTF-tailored multiscale fusion of high-resolution MS and Pan imagery," *Photogramm. Eng. Remote Sens.*, vol. 72, no. 5, pp. 591–596, May 2006.

[5] A. Toet, "Image fusion by a ratio of low pass pyramid," *Pattern Recog. Lett.*, vol. 9, no. 5, pp. 245–253, May 1989.

[6] J. Lee and C. Lee, "Fast and efficient panchromatic sharpening," *IEEE Trans. Geosci. Remote Sens.*, vol. 48, no. 1, pp. 155–163, Jan. 2010.

[7] A. Michelson, *Studies in Optics*. Chicago, IL, USA: Univ. Chicago Press, 1927.

[8] E. Peli, "Contrast in complex images," *J. Opt. Soc. Amer. A*, vol. 7, no. 10, pp. 2032–2039, Oct. 1990.

[9] B. Aiazzi, L. Alparone, S. Baronti, I. Pippi, and M. Selva, "Generalised Laplacian pyramid-based fusion of MS+ P image data with spectral distortion minimisation," *ISPRS Int. Archives Photogramm. Remote Sens.*, vol. 34, no. 3A-W3, pp. 3–6, 2002.

[10] T.-M. Tu, P. S. Huang, C.-L. Hung, and C.-P. Chang, "A fast intensity-hue-saturation fusion technique with spectral adjustment for IKONOS imagery," *IEEE Geosci. Remote Sens. Lett.*, vol. 1, no. 4, pp. 309–312, Oct. 2004.

[11] B. Aiazzi, S. Baronti, and M. Selva, "Improving component substitution pansharpening through multivariate regression of ms+pan data," *IEEE Trans. Geosci. Remote Sens.*, vol. 45, no. 10, pp. 3230–3239, Oct. 2007.

[12] T. Tu, S.-C. Su, H.-S. Shyu, and P.-S. Huang, "A new look at IHS-like image fusion methods," *Inf. Fusion*, vol. 2, no. 3, pp. 177–186, Sep. 2001.

[13] T. Ranchin and L. Wald, "Fusion of high spatial and spectral resolution images: the ARSIS concept and its implementation," *Photogram. Eng. Remote Sens.*, vol. 66, no. 1, pp. 49–61, Jan. 2000.

[14] A. Garzelli and F. Nencini, "Interband structure modeling for pan-sharpening of very high-resolution multispectral images," *Inf. Fusion*, vol. 6, no. 3, pp. 213–224, Sep. 2005.

[15] J. Nunez, X. Otazu, O. Fors, A. Prades, V. Pala, and R. Arbiol, "Multiresolution-based image fusion with additive wavelet decomposition," *IEEE Trans. Geosci. Remote Sens.*, vol. 37, no. 3, pp. 1204–1211, May 1999.

[16] L. Alparone, L. Wald, J. Chanussot, C. Thomas, P. Gamba, and L. Bruce, "Comparison of pansharpening algorithms: Outcome of the 2006 GRS-S data-fusion contest," *IEEE Trans. Geosci. Remote Sens.*, vol. 45, no. 10, pp. 3012–3021, Oct. 2007.

[17] L. Alparone, S. Baronti, A. Garzelli, and F. Nencini, "A global quality measurement of pan-sharpened multispectral imagery," *IEEE Geosci. Remote Sens. Lett.*, vol. 1, no. 4, pp. 313–317, Oct. 2004.

[18] X. Otazu, M. Gonzalez-Audicana, O. Fors, and J. Nunez, "Introduction of sensor spectral response into image fusion methods. application to wavelet-based methods," *IEEE Trans. Geosci Remote Sens.*, vol. 43, no. 10, pp. 2376–2385, Oct. 2005.